Wind-driven inner-shelf circulation off central Oregon during summer

Anthony R. Kirincich and John A. Barth
College of Oceanic and Atmospheric Sciences, Oregon State University, Corvallis, Oregon, USA

Brian A. Grantham
Washington State Department of Ecology, Coastal and Estuarine Assessment Unit, Olympia, Washington, USA

Bruce A. Menge and Jane Lubchenco
Department of Zoology, Oregon State University, Corvallis, Oregon, USA

Received 20 July 2004; revised 10 February 2005; accepted 14 March 2005; published 11 October 2005.

[1] Velocity measurements from 17 deployments of moored acoustic Doppler current profilers obtained during four summer upwelling seasons are used to describe the cross-shelf divergence of Ekman transport in the inner shelf off Oregon. For each deployment the measured surface and bottom cross-shelf transports were compared with estimates of the theoretical Ekman transports to find the fraction of full theoretical Ekman transport present. In general, in 15 m of water at 1–2 km offshore, measured transport was 25% of the full Ekman transport. Measured transports reached full Ekman transport 5–6 km offshore in 50 m of water. This result indicates that the region of active upwelling marked by the divergence of Ekman transport was limited to a narrow region along the coast. With small wind stress curl and no major headlands in the region, no along-shelf trends in the transport fractions were observed. Average transport fractions at each station were similar from year to year with one exception. The interannual variability seen at this particular site was most likely a result of local along-shelf bathymetric features. In addition, a weak linear relationship was found between the ambient stratification and the fraction of full Ekman transport. Reduced cross-shelf transport occurred at times of decreased stratification. This type of "shutdown" of the inner-shelf cross-shelf circulation has significant biological implications, sequestering production in the nearshore and reducing larval cross-shelf transport.

Citation: Kirincich, A. R., J. A. Barth, B. A. Grantham, B. A. Menge, and J. Lubchenco (2005), Wind-driven inner-shelf circulation off central Oregon during summer, *J. Geophys. Res.*, *110*, C10S03, doi:10.1029/2004JC002611.

1. Introduction

[2] The cross-shelf circulation associated with coastal upwelling has been well documented for wind-driven middle and outer continental shelves, where water depths are generally deeper than 50 m. Numerous review papers exist on the subject [i.e., *Huyer*, 1983, 1990; *Hickey*, 1998] and the interactions of the wind forcing, surface and bottom transports, and bottom stress from these phenomena have been documented on many of the world's continental shelves [i.e., *Allen and Smith*, 1981; *Smith*, 1995]. In general, all describe a cross-shelf circulation with offshore surface Ekman transport driven by the along-shelf wind stress. A return flow exists either in the interior of the fluid or in the bottom boundary layer (BBL) created by the interaction of the along-shelf current and the shelf bottom. The contributions of the interior and BBL to the return flow over the middle to outer shelf is dictated by the slope Burger number, a measure of the relative importance of stratification and bottom slope [*MacCready and Rhines*, 1993; *Austin and Lentz*, 2002]. Most middle and outer shelf investigations of upwelling have found fully developed Ekman transport in the boundary layers with small stresses in the interior [*Lentz*, 1992; *Lentz and Trowbridge*, 1991]. Less is known about downwelling circulation, although observational [*Winant*, 1980] and model studies [*Austin and Lentz*, 2002; *Allen et al.*, 1995] confirm the same notion of wind-forced onshore Ekman transport and offshore compensatory flow beneath.

[3] Inshore of these middle and outer shelf locations exists a region in which the wind-driven cross-shelf Ekman transport is reduced in magnitude due to the presence of a coastal wall [*Gill*, 1982]. The cross-shelf extent of this divergence of Ekman transport encompasses the region of active upwelling or downwelling [*Lentz*, 2001] and is bounded offshore by the upwelling or downwelling front. Further, using a numerical model *Allen et al.* [1995] found a large fraction of upwelling takes place in relatively shallow water near the coast. Their results showed that half of the

0148-0227/05/2004JC002611$09.00

upwelled water came directly from the BBL in shallow water inshore of 20 m depth. In this area, surface and bottom boundary layers occupy the entire water column [*Lentz*, 1995]. Thus on wind-driven shelves the inner shelf serves as a transition zone between the middle and outer shelf, where wind forcing and large-scale pressure gradients are dominant forces, and the nearshore where surface gravity wave radiation stresses are large.

[4] A number of recent investigations have attempted to document the nature of cross-shelf circulation in the inner shelf. In 30 m of water off central California, *Lentz* [1994] identified a cross-shelf surface flow driven by along-shelf winds and a bottom return flow driven by the along-shelf jet. In *Lentz*'s [1994] study area, flow was found to be essentially two dimensional, with no significant depth-averaged cross-shelf flow [*Lentz*, 1994]. Using a cross-shelf array of moorings on the wide, gently sloping North Carolina shelf, *Lentz* [2001] observed cross-shelf transport increased moving offshore as dictated by Ekman theory. He reported large differences in cross-shelf transports between summer, when waters were more stratified, and fall, when waters were only weakly stratified. Demonstrating stratification's effect on transport, *Allen et al.* [1995] showed the majority of upwelling occurred within 3 km of the coast when stratification was present, and within 8 km of the coast when no stratification was present. *Austin and Lentz* [2002] obtained similar results, finding that cross-shelf transports in the inner shelf decreased as stratification was reduced.

[5] Summarizing these previous works, circulation in this shallow area is dependent on wind forcing, but can be significantly influenced by stratification. The link between the level of stratification and the amount of cross-shelf Ekman transport exists because reducing the stratification increases the eddy viscosity (A_v), which increases the Ekman layer depth (d) as $d = \sqrt{2A_v/f}$, where f is the Coriolis parameter. For shallow water near the coast, less of the Ekman spiral is realized when stratification is reduced, leading to a reduction in cross-shelf transport. This type of reduction (or shutdown) of cross-shelf circulation as a result of reduced stratification in the inner shelf affects the circulation dynamics of the entire shelf [*Lentz*, 2001; *Samelson*, 1997] and may be important for biological processes as well. In particular, understanding patterns of cross-shelf circulation is key to understanding the processes responsible for transport of larvae and particulates (phytoplankton and detritus) to and from benthic coastal habitats [*Morgan*, 2001].

[6] The study described here analyzes the cross-shelf circulation in the narrow, steeply sloping inner shelf along the coast of central Oregon. Located on the eastern boundary of the North Pacific Ocean, the shelf-wide upwelling system off Oregon has been well documented [*Allen and Smith*, 1981; *Huyer*, 1983] and is known for its high productivity [*Small and Menzies*, 1981]. During summer, southward winds with mean values of 0.03 N m^{-2} and small offshore wind stress curl [*Samelson et al.*, 2002] drive offshore surface flow, upwelling, and an along-shore equatorward jet with mean velocities reaching 0.25 m s^{-1} [*Huyer*, 1983]. Shelf waters off Oregon are generally highly stratified with top to bottom density differences as large as 2 kg m^{-3} regularly occurring [*Huyer*, 1983]. For the most part, these shelf studies have left the inner shelf off Oregon poorly resolved. However, since 1999 the Partnership for Interdisciplinary Studies of Coastal Oceans (PISCO) program has collected numerous long-term hydrographic and velocity measurements in the inner shelf along the central Oregon coast.

[7] The PISCO program is a long-term ecological consortium created in 1998 to study the link between inner-shelf oceanography and marine ecosystems along the U.S. west coast. The objectives of the program are to quantify patterns of distribution, abundance, and diversity in nearshore communities and determine how oceanographic processes influence these patterns. This study begins to quantify the wind-driven dynamics in the inner shelf, forming a foundation for interdisciplinary analyses to follow. A companion paper by J. A. Austin and B. A. Grantham (Subinertial variability of the Oregon inner shelf, submitted to *Journal of Geophysical Research*, 2005, hereinafter referred to as Austin and Grantham, submitted manuscript, 2005) uses different portions of the PISCO data set to analyze subinertial along-shelf and cross-shelf variability in the inner shelf off Oregon. In summary, the PISCO project has enabled the transition between shelf and nearshore circulation occurring within the inner shelf to be more clearly understood.

[8] Using measurements obtained from the long-term mooring efforts taking place in the region, this study describes the offshore extent of the Ekman divergence off Oregon by comparing the measured cross-shelf transports to theoretical values. The observations used in this study are introduced in section 2, along with the theory and data analysis techniques employed to compute the measured and theoretical Ekman transports. Section 3 describes the results of the transport fraction calculation and then examines the effects of both stratification and the frictional coefficient used to obtain bottom stress. A discussion of the key results follows in section 4, including a comparison with previous results from the wide, gently sloping North Carolina shelf. Section 5 summarizes the findings of this study.

2. Data and Methods

2.1. Data Sources

[9] The bulk of the observations used here were made as part of PISCO's Oregon State University (OSU) mooring program. This mooring component of the larger PISCO program has collected hydrographic measurements in Oregon's inner shelf each summer since 1998. Data from years 1999, 2001, 2002, and 2003 are examined here while similar measurements from years 1998, 1999, and 2000 are presented by Austin and Grantham (submitted manuscript, 2005). Over the course of the four summers examined here, the program made 14 deployments of bottom-mounted upward looking acoustic Doppler current profilers (ADCPs) at six locations spanning an along-shelf distance of 83 km (Figures 1 and 2). The ADCPs, 600 kHz Workhorse Broadband Sentinels from RD Instruments, collected 2 min averages of water velocities from 1 m depth increments starting 3 m above the seafloor. Adjacent to each ADCP deployment, a separate mooring recorded temperature at multiple depths and conductivity at midwater. These instruments sampled every 2–30 min, depending on the instrument and deployment year.

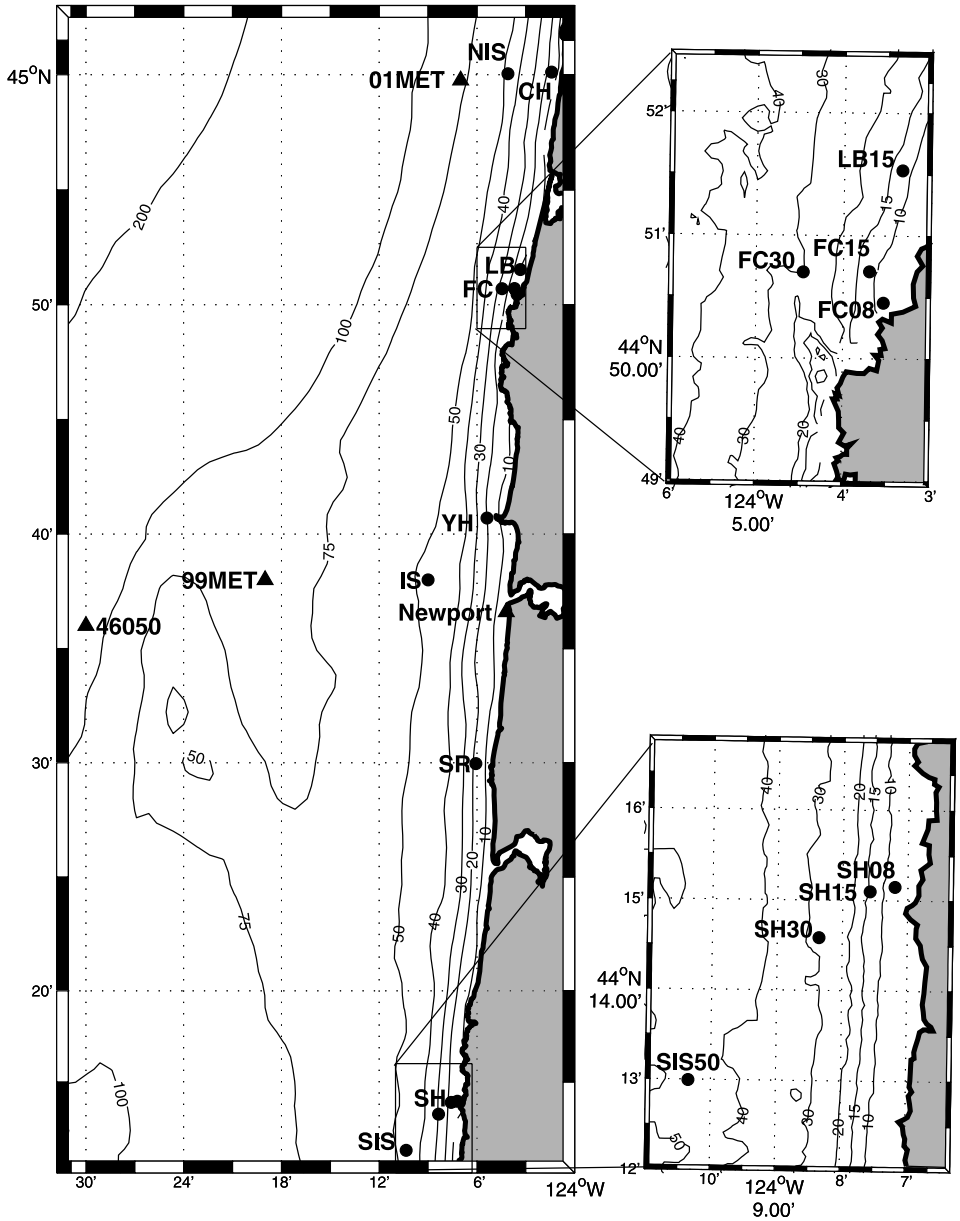

Figure 1. Study region: the continental shelf off Oregon along the west coast of the United States. The locations of all acoustic Doppler current profiler (ADCP) deployments are shown as filled circles near their station ID. Wind measurements from buoy 46050 (46050), the Newport CMAN station (Newport), the NOPP 1999 meteorological buoy (99MET), and the COAST 2001 meteorological buoy (01MET) are marked by triangles. Isobaths are in 10 m increments up to 50 m. Additionally, the 15 m isobath is included in both insets for reference.

[10] The deployed ADCP array varied in size and locations among the years described. Mean water depths for the deployments ranged from 8 to 30 m, although most were located at 15 m (Table 1, Figure 3). While only one deployment occurred in 1999 at station YH at 15 m of water, five were made in 2001, with two measurement intervals at 15 m at station CH separated by 20 days, and 8 m and 15 m deployments at both stations FC and SH. In 2002, 15 m deployments occurred at stations FC (two measurement intervals separated by 20 days), SR, and SH, while shorter 30 m deployments were also made at stations FC and SH. The array was reduced in 2003, with 15 m deployments at stations LB (near FC), SR, and SH only.

[11] To augment the PISCO array with offshore observations, 3 additional velocity measurements from adjacent field programs are included in this study. Velocity profiles were obtained from a 1999 deployment at station IS, located offshore and 5 km south of station YH (Figure 1), as part of the Prediction of Wind-Driven Coastal Circulation Project, a NOPP Project [*Boyd et al.*, 2000; *Oke et al.*, 2002]. Similar deployments were made in 2001 as part of the Coastal Ocean Advances in Shelf Transport (COAST) Project

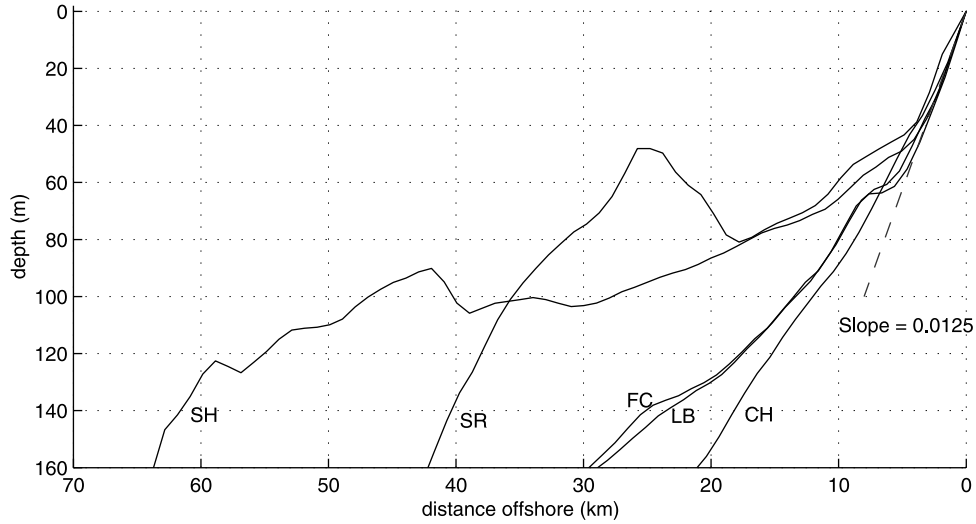

Figure 2. Bottom profiles from all major PISCO mooring locations plotted on the axis of offshore distance in kilometers. The station ID is near each profile. Plotted on this axis, the profiles line up with the southernmost station (SH) on the left and with the northernmost station (CH) profile on the right. A dashed line representing a bottom slope of 0.0125 is included for reference.

offshore of stations CH and SH [*Boyd et al.*, 2002]. Each of these three deployments, all at 50 m depth, consisted of moored upward looking 300 kHz RDI Workhorse Broadband ADCPs, collecting 2 min ensemble averages in 2 m bins starting at 8 m above the seafloor.

[12] Observations from a number of buoy and coastal stations were used to estimate the wind velocities at each mooring location. Hourly averages of wind measurements from the NOAA National Data Buoy Center's (NDBC) buoy 46050 and the Newport, Oregon NOAA Coastal Marine Automated Network (CMAN) station NWPO3 are examined in this study. The CMAN station is located on the south jetty of the Newport harbor entrance while buoy 46050 is located 33 km west of Newport in 100 m of water (Figure 1). In addition, hourly averages of wind measurements obtained by meteorological buoys operated by the 1999 NOPP program and the 2001 COAST program were taken into consideration as midshelf estimates of wind velocity during those years (Figure 1). Wind velocities are not measured as part of the PISCO program.

2.2. Ekman Transport Theory

[13] The wind-driven cross-shelf circulation can be described by the relationship between the cross-shelf transport and the applied stress that drives it. Starting from a linear, layer-integrated along-shelf momentum balance,

$$\frac{\partial V}{\partial t} + fU = -\frac{1}{\rho_o}\frac{\partial P}{\partial y} + \frac{\tau_s^y}{\rho_o} - \frac{\tau_b^y}{\rho_o}, \tag{1}$$

where V, U, and P are the layer integrated along-shelf velocity, cross-shelf velocity, and pressure, ρ_o is a reference density, and τ_s^y and τ_b^y are the applied stresses at the surface (s) and the bottom (b) of the layer. Assuming steady flow with no pressure gradient or bottom friction, equation (1) reduces to the Ekman transport equation:

$$U = \frac{\tau_s^y}{\rho_o f}, \tag{2}$$

defined as the cross-shelf transport balanced by the applied surface stress divided by a reference density and the Coriolis parameter [*Ekman*, 1905]. In shallow waters, where this Ekman transport is not fully developed, the relationship can be further approximated using a linear regression as [*Lentz*, 2001]

$$U = a\frac{\tau_s^y}{\rho_o f} + b, \tag{3}$$

Table 1. Mean, Standard Deviation, and Principal Axis for All ADCP Deployments[a]

Station	Depth, m	Duration, days	μ_{east}, m s^{-1}	σ_{east}, m s^{-1}	μ_{north}, m s^{-1}	σ_{north}, m s^{-1}	θ_p	Range of θ_p
				1999				
YH	15	67	−0.007	0.004	0.014	0.013	13	6
IS	50	77	0.005	0.004	0.004	0.014	12	8
				2001				
CH_a	15	80	−0.012	0.003	−0.068	0.013	11	12
CH_b	15	50	−0.014	0.003	−0.067	0.009	13	16
NIS	50	104	−0.007	0.004	−0.011	0.017	9	3
FC	08	100	−0.021	0.005	−0.015	0.004	−28	71
FC	15	62	−0.0038	0.002	−0.017	0.007	5	80
SH	08	46	−0.033	0.003	−0.081	0.017	7	1
SH	15	63	−0.007	0.002	−0.077	0.014	6	4
SIS	50	105	0.015	0.003	−0.013	0.011	5	10
				2002				
FC_a	15	62	−0.019	0.004	−0.001	0.008	22	43
FC_b	15	33	−0.017	0.002	−0.001	0.005	22	21
FC	30	51	−0.029	0.004	−0.001	0.014	13	43
SR	15	115	0.002	0.002	0.002	0.012	4	15
SH	15	111	0.000	0.002	−0.054	0.014	5	7
SH	30	52	0.009	0.002	0.02	0.015	5	10
				2003				
LB	15	111	−0.02	0.005	−0.064	0.011	21	7
SR	15	116	−0.002	0.002	0.000	0.012	5	9
SH	15	122	−0.003	0.002	−0.049	0.015	5	8

[a]Mean (μ) and standard deviation (σ) of both north and east velocities are in m s^{-1}. The calculated principal axis directions (θ_p) are clockwise from true north. The range of θ_p direction with depth is also included.

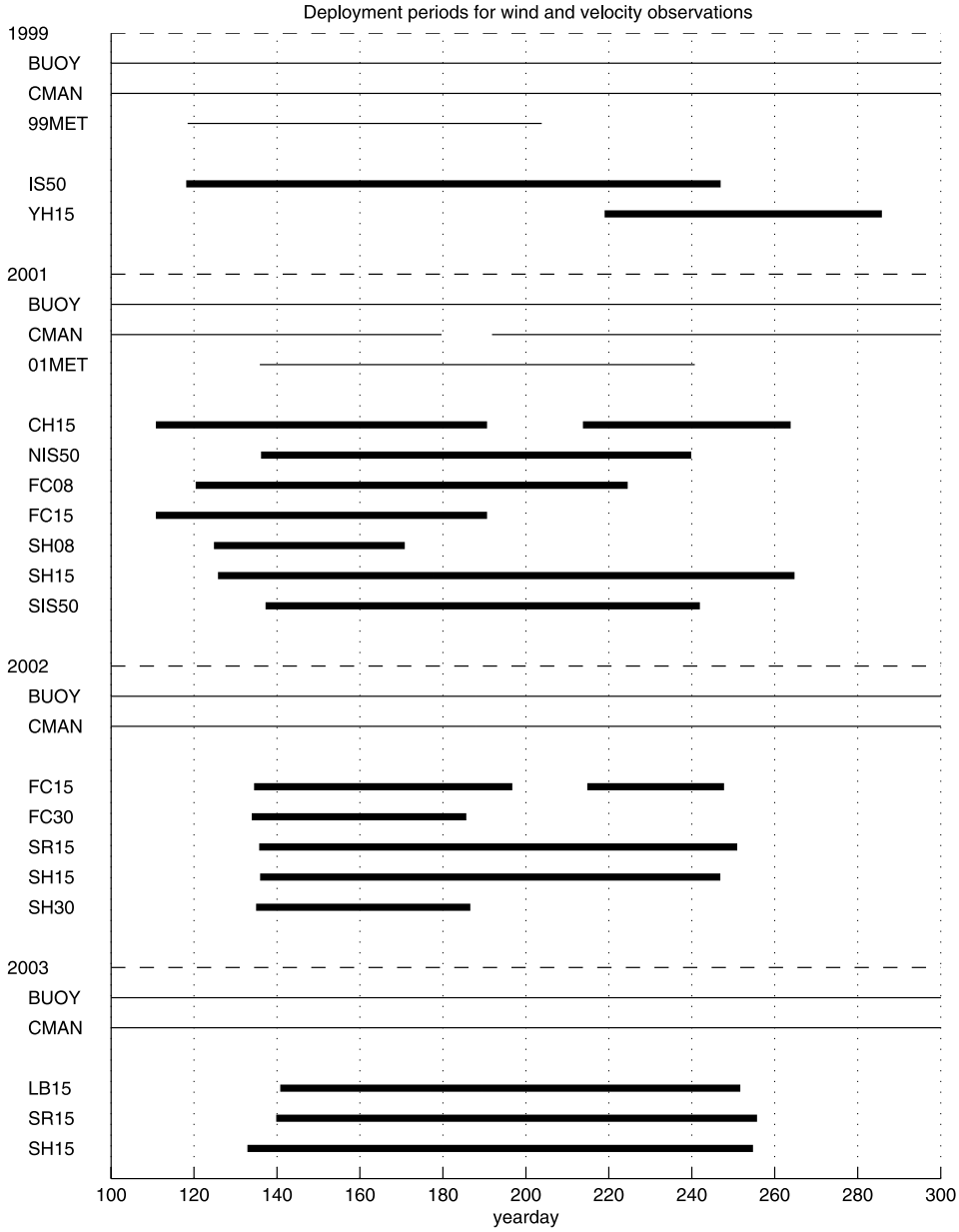

Figure 3. Deployment periods of ADCP (bold lines) and wind measurements (thin lines) used in this study.

with a, the slope of the line, defining the fraction of full Ekman transport present while b, the y intercept, is the transport at zero wind stress. Using this relationship for the surface Ekman layer, and a similar one for the bottom layer, we can calculate how measured surface and bottom transports compare with the full theoretical Ekman transports computed from the surface and bottom stresses.

[14] Evaluating (3) is best handled using a neutral regression technique [*Garrett and Petrie*, 1981]. While a normal linear regression technique minimizes the variance in one dimension, a neutral regression minimizes the variance in both dimensions. Here, the regression coefficient (a) is defined as the square root of the ratio of the variance of the second time series to the variance of the first time series, or

$$a = \left(\frac{\sigma_2^2}{\sigma_1^2}\right)^{1/2}. \tag{4}$$

More complex methods for computing this regression exist [e.g., *Reed*, 1992], however these methods differ from (4) only if known measurement uncertainties are used to compute the required weighting functions. If the variance of the input time series are used as weights, a reasonable assumption if measurement uncertainties are not known [*Reed*, 1992], this method collapses to the simple ratio used by *Garrett and Petrie* [1981].

[15] Using these methods we can define the offshore extent of Ekman divergence using the theoretical Ekman transport given by (2) and the measured Ekman transports derived from the velocity observations (see next section). Here, the neutral regression coefficient is the square root of the ratio of the measured Ekman transport (time series 2) to the theoretical Ekman transport (time series 1).

2.3. Calculating Ekman Transports

2.3.1. Measured Ekman Transport

[16] For each deployment, estimates of the cross-shelf transport in the surface and bottom Ekman layers were calculated from the cross-shelf velocity profiles obtained from the ADCPs. As ADCPs do not sample the entire water column, the cross-shelf velocity profiles were extrapolated to the surface and bottom in order to compute cross-shelf transports occurring throughout the water column. For the COAST 50 m deployments in 2001, velocity observations below 40 m and above 6 m depth were excluded because of quality control concerns [*Boyd et al.*, 2002]. For station IS in 1999, velocity observations below 40 m and above 8 m were excluded from the velocity profiles [*Boyd et al.*, 2000].

[17] Similar "tide-independent" quality control analysis at the PISCO deployment locations would exclude up to 1/3 of the water column at high tide due to larger tidal height variations at these shallow locations. Therefore profiles of the total acoustic backscatter intensity were used to create "tide-following" velocity profiles for all of the 30, 15, and 8 m ADCP deployments. Produced for each ensemble by summing the backscatter intensity profiles of all four beams, the depth of the maximum total backscatter intensity was marked as the water surface. Velocities from all depth bins above this surface were masked. An additional surface bin of the measured water velocities was subtracted from the masked profiles at 8 and 15 m locations due to side lobe reflection [*Gordon*, 1996]. For the same reason, an additional three surface bins were subtracted from the 30 m location velocity profiles. All further analysis was performed on hourly averages of the tide-following velocity profiles from the PISCO deployments and the quality controlled 50 m deployments mentioned above.

[18] Possible sources of error in ADCP measurements include both random error and a bias due to surface gravity wave orbital velocities. RDI literature [*Gordon*, 1996] estimates the random error in the velocity measurements as the standard deviation of the difference in the vertical velocity estimates made by the two beam pairs. This "error" velocity can then be estimated for each depth bin measured for each deployment. Error velocities averaged 0.01 m s^{-1} for all PISCO deployments and less than 0.01 m s^{-1} for the COAST and NOPP deployments [*Boyd et al.*, 2000, 2002]. In addition, because most deployments were in relatively shallow water, the inclusion of partial periods of the dominant surface gravity waves in the 2 min ensemble averages might cause a bias in the velocity estimates. An estimate of this type of bias can be made considering the particle motion of a 1 m amplitude linear wave. On the basis of these parameters the estimated bias ranged from 0 to a maximum of 0.025 m s^{-1} for wave periods from 4 to 20 s. In 15 m of water, the range of the maximum possible bias with depth was less than 0.01 m s^{-1}. Thus the bias is a strong function of wave period but a weaker function of depth below the surface, as the majority of the bias is absorbed into the depth-averaged mean velocity. Since we are only concerned with the depth-dependent component of the water velocities, the maximum possible bias due to surface gravity waves is of similar magnitude as the random error given above.

[19] The principle axis coordinate system was used for velocity observations presented here. The principal axis of flow is that which minimizes the velocity variances in the minor axis. For most deployments, orientations of the axes ranged from 4° to 13° clockwise from north (Table 1), with notable exceptions located primarily at station FC. In general, the principal axes are aligned with local bathymetric contours. After rotation into the principal axis coordinate system, the velocity profiles were considered to be in along-shelf and across-shelf coordinates. Cross-shelf transports were then found from the cross-shelf components of the measured water velocity profiles.

[20] To compute transports based on the full water column, a number of extrapolation techniques were considered. The simplest method, vertically extrapolating to the surface and the bottom assuming a constant velocity between the nearest measurements and the boundary, was attempted for all deployments (Figure 4). For 8 m and 15 m deployments, 1 m of extrapolation was needed at the surface and 2 m at the bottom, while for the 30 m deployments velocities were extrapolated 3 m at the surface and 2 m at the bottom. Extrapolated distances at 50 m were much larger as noted earlier. For the 8 m and 15 m deployments, only the constant velocity method was considered because the extrapolated distances were small. Given the larger distances between the nearest measurements and the surface or bottom at the 30 m and 50 m locations, two alternative profiles were considered. The first assumed a constant velocity slope between the two highest measurements and the water surface for the top portion, and a constant velocity slope between the deepest velocity measurement and 0 m s^{-1} at the bottom (Figure 4). However, it is possible that the true shape of the velocity profiles includes a surface mixed layer with no vertical shear [*Lentz*, 1992]. Thus the second alternative was a combination of the constant velocity extrapolation to surface and the constant slope extrapolation to the bottom (Figure 4). After extrapolation, the depth-averaged mean of the cross-shelf circulation was removed from all deployments to isolate the depth-dependent cross-shelf circulation.

[21] In this analysis, the flow field was assumed to be two dimensional and uniform in the along-shelf direction. The inner shelf off the coast of central Oregon is relatively along-shelf uniform in nature (Figures 1 and 2). While the large Heceta Bank in the southern part of the region influences circulation at depths greater than 50 m, there is little variation in along-shelf bathymetry at depths less than 50 m (Figure 2). However, small-scale coastal topography could become an influencing factor in areas immediately adjacent to the coastline (Figure 1). If the two-dimensional assumption used in this calculation is valid, the total cross-shelf transport caused by wind forcing should have zero mean. Therefore the depth-averaged portion of the cross-shelf transport is expected to be small and uncorrelated with the wind. This criterion will be tested in section 3.

[22] From the resulting zero-mean hourly profiles for each deployment, the surface transport was found by vertically integrating from the surface down to the first zero

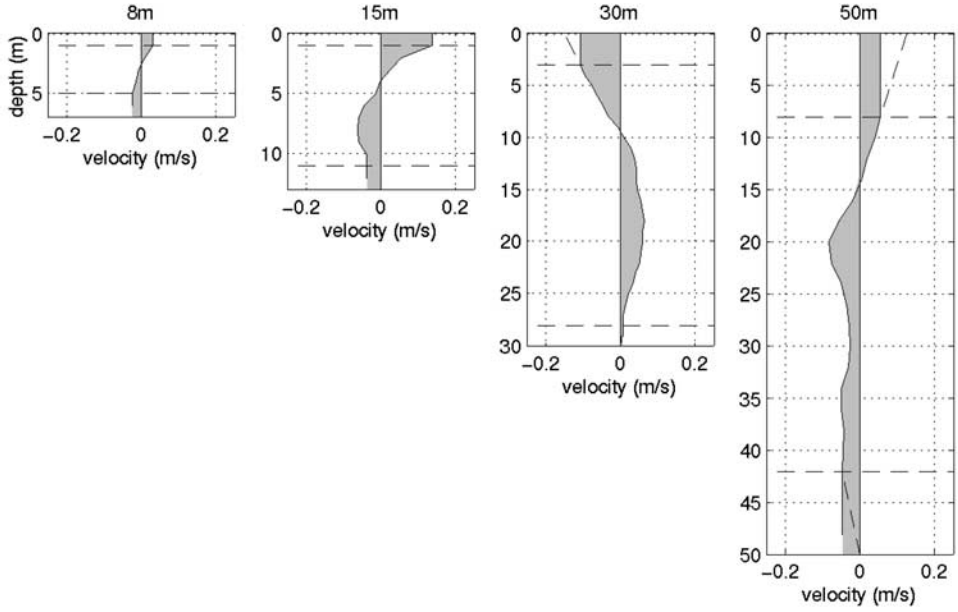

Figure 4. Examples of hourly averaged cross-shelf velocity profiles for each deployment depth. In each the measured velocities exist between the horizontal dashed lines. These cross-shelf profiles were used to calculate measured surface and bottom transports following the methods described in the text. The shaded areas of these profiles form the measured surface or bottom transports using the constant velocity extrapolation method. Constant slope extrapolations are included in the 30 m and 50 m deployments for reference.

crossing of the profile (Figure 4). Similarly, the bottom transport was found by vertically integrating from the bottom up to the lowest zero crossing available. These integrated transports form the measured surface and bottom transports used in the calculation. This method has been used previously for both inner-shelf [*Lentz*, 2001; *Austin and Lentz*, 2002] and outer-shelf [*Allen et al.*, 1995] analysis.

2.3.2. Theoretical Ekman Transport

[23] Estimates of the surface and bottom stresses were used to calculate the theoretical Ekman transports in each layer using equation (2). For all deployments, a reference density of $\rho_o = 1025$ kg m^{-3} and a Coriolis parameter of $f = 1.03 \times 10^{-4}$ s^{-1} corresponding to a latitude of 45° are used. The along-shelf wind stress was calculated from observed wind velocities at each measurement location described earlier. The hourly averages of all available wind measurements were rotated into the principal axes coordinate system defined for each ADCP deployment. These estimates of along-shelf and cross-shelf wind velocities were used to compute wind stress in the along-shelf direction using the empirical method given by *Large and Pond* [1981]:

$$\tau_s^y = \rho_a C_f |\mathbf{v}| v, \tag{5}$$

where $\rho_a = 1.25$ kg m^{-3} and C_f, the frictional drag coefficient, is a function of wind speed as well as the height of the measurement. All measurements were translated to 10 m height wind velocities and wind stresses using the assumption of a stable atmosphere [*Large and Pond*, 1981].

[24] Using the neutral regression technique outlined above, the along-shelf wind stress observed offshore at buoy 46050 during each summer was compared with wind stresses from the Newport CMAN station and the midshelf meteorological moorings in 1999 and 2001 to find the most representative wind for each deployment. Curiously, the magnitude of the buoy 46050 along-shelf wind stress matched by the CMAN station varies somewhat year to year (Table 2). In 1999, 2001, and 2003, CMAN station

Table 2. Comparison of Along-Shelf Wind Stress at Buoy 46050, the Newport CMAN Station, and the Midshelf Meteorological Buoys Using the Neutral Regression Technique[a]

Stations Compared	Year Day Start	Year Day End	Fraction	CC	Cross-Shelf Wind Stress Curl $\nabla \times \tau^y$, 10^{-6} N m^{-3}
			1999		
Buoy/CMAN	100	250	0.77 ± 0.13	0.93	1.3
Buoy/midshelf	118	204	0.72 ± 0.06	0.98	0.8
Midshelf/CMAN	118	204	1.09 ± 0.17	0.93	0.4
			2001		
Buoy/CMAN	136	241	0.77 ± 0.17	0.93	0.7
Buoy/midshelf	136	241	0.68 ± 0.09	0.96	1.2
Midshelf/CMAN	136	241	1.14 ± 0.23	0.93	−0.3
			2002		
Buoy/CMAN	100	250	0.91 ± 0.14	0.87	0.4
			2003		
Buoy/CMAN	100	250	0.79 ± 0.13	0.87	0.4

[a]The correlation coefficients (CC) between each pair are also shown, with all correlations being significant at the 95% confidence level. As an example, regressing buoy 46050 and the CMAN station in 1999 yielded 0.77, meaning that the along-shelf wind stress at the CMAN station was 77% of the magnitude of the wind stress measured at buoy 46050 to the 95% confidence interval cited. Estimates of the average cross-shelf wind stress curl ($\times 10^{-6}$) between the measurement locations for each year are included as well.

along-shelf wind stress was ~80% of the wind stress found offshore at buoy 46050. However, in 2002 wind stress at the CMAN station was closer (~90%) to the wind stress at the offshore buoy. In 1999 and 2001, the regression of the midshelf winds to the offshore buoy winds is similar in magnitude to the regression between CMAN winds and buoy winds. In fact, winds at midshelf locations were found to be statistically equal to CMAN winds at Newport.

[25] From the comparisons shown, the CMAN station winds should be most representative of local winds at the 8, 15, and 30 m mooring deployments during the summer periods of interest and will be used in this analysis for those stations (Table 2). Further, given the high correlation between midshelf winds and CMAN winds in both 1999 and 2001, for continuity the CMAN winds will be used for the 50 m deployments as well.

[26] While these regressions give estimates of cross-shelf curl of the along-shelf wind stress, the average cross-shelf wind stress curl along the Oregon coast was also computed. Curl-driven upwelling can be a significant part of the total upwelling [*Pickett and Paduan*, 2003], yet as stated earlier, *Samelson et al.* [2002] reported a small wind stress curl off central Oregon. With a maximum computed cross-shelf curl of 10^{-6} N m^{-3}, our calculations agree with these conclusions. In addition, most of the wind stress curl found occurred offshore of the midshelf moorings at 80 m depth (Table 2). This is an important result, as it implies that a divergence of Ekman transport inshore of 80 m depth is most likely caused by coastal upwelling rather than curl-driven upwelling. For these reasons, wind stress curl is not considered to be an important factor here.

[27] The along-shelf bottom stress was approximated, following *Lentz* [2001] as

$$\tau_b^y = \rho_o r v_b, \tag{6}$$

where v_b is taken as the along-shelf bottom velocity (i.e., the deepest measured along-shelf velocity during each deployment), and r is the frictional coefficient. A value of $r = 5 \times 10^{-4}$ m s^{-1} was used here based on previous midshelf observations [*Lentz*, 2001; *Lentz and Winant*, 1986]. While a quadratic stress parameterization is thought to be more appropriate in and near the surf zone [*Feddersen et al.*, 1998], initial tests found correlations of measured and theoretical transports calculated using linear bottom stress were not significantly different than correlations of measured and theoretical transports calculated using quadratic bottom stress. Thus for simplicity, quadratic bottom stress was not considered here. In contrast, the success of the bottom transport fraction calculation is quite sensitive to the frictional coefficient used. This parameter is evaluated further in section 3.2.

[28] Finally, prior to performing the neutral regression both the measured and theoretical transports were low-pass filtered using a filter with a 40 hour cutoff [*Mooers*, 1968] in order to isolate the subtidal portions of the transport calculations. Further, in the results shown below the 95% confidence level is used throughout to establish significant correlations and confidence intervals.

2.4. Hydrographic Observations

[29] Hydrographic observations from moorings adjacent to each 15 m ADCP location were used in this study to examine the role of stratification on cross-shelf transport. A typical mooring at 15 m in the PISCO mooring program consists of temperature measurements at 1, 4, 9, and 14 m, with additional temperature and salinity measurements at 8 m. All temperature and salinity records were low-pass filtered using the method described above to isolate the subtidal frequencies of variability. However, the PISCO data set lacks adequate vertical salinity coverage to compute stratification using the top to bottom density difference. Therefore the difference between the surface and bottom temperature sensors, divided by the distance between them, is used as a proxy for the stratification. The majority (60%) of surface temperature values were from 1 m depth. When 1 m measurements were not available, temperature measurements from 4 m depth were substituted. The validity of using the temperature gradient as a proxy for the density stratification is discussed in section 4.4.

3. Results

3.1. Transport Results

[30] Using the methods described above, the measured and theoretical transports for both the surface and bottom layers were calculated for each deployment and then compared using the neutral regression technique. The results of this regression indicate the fraction of theoretical surface or bottom Ekman transport present, and results from all deployments are listed in Table 3. Significant results are defined here as those deployments where the measured and theoretical transports are positively correlated, while the wind stress and the depth-averaged velocity are uncorrelated. Both criteria indicate that the assumption of along-shelf uniformity is valid for the wind-driven circulation. On the basis of these conditions, significant results were found for the majority of the 17 deployments (Table 3). The necessary criteria were met for the surface layer at 10 15 m deployments, one 30 m deployment, and all 50 m deployments. Significant results for the bottom layer were found only during nine 15 m deployments and two 50 m deployments. It is of interest to note that both 8 m locations failed the necessary conditions for significance. Many of the intercepts, b, were not significantly different than zero, indicating that cross-shelf transport was small in the absence of stress. Among the significant results, b increases moving offshore in the surface layer from an average of 0.05 m^2 s^{-1} at 15 m to 0.2 m^2 s^{-1} at 50 m. In the bottom layer, mean transports are in the opposite direction, increasing offshore from 0.02 m^2 s^{-1} at 15 m to 0.12 m^2 s^{-1} at 50 m. These transports represent processes in the momentum balance (1) that we have assumed to be small (e.g., along-shelf pressure gradients or accelerations), the importance of which apparently increases moving offshore. However, as our focus is on wind-driven cross-shelf circulation, these non-wind-driven mean transports will not be discussed further.

[31] Comparing the different methods of extrapolation used for the 30 m and 50 m deployments showed the following. At the two 30 m locations, the average difference in transport fractions between the three methods was less than 3%. Thus only results using constant velocity extrapolation profiles are included in Table 3 for simplicity. At the three 50 m locations, transport fractions found using the two alternative profiles differed from the constant velocity

Table 3. Results of the Ekman Transport Fraction Calculation[a]

Station	Depth, m	Surface Transport, $m^2\ s^{-1}$		Bottom Transport, $m^2\ s^{-1}$		Transport Ratio
		a	*b*	*a*	*b*	
			1999			
YH	15	0.34 ± 0.086	0.05 ± 0.030	0.27 ± 0.073	0.00 ± 0.028	0.79
IS_{vel}	50	1.09 ± 0.254	0.19 ± 0.106	1.03 ± 0.193	−0.11 ± 0.082	0.95
IS_{slope}	50	1.27 ± 0.278	0.09 ± 0.116	0.91 ± 0.172	−0.05 ± 0.079	0.72
IS_{combo}	50	1.10 ± 0.277	0.23 ± 0.106	0.84 ± 0.172	0.00 ± 0.079	0.76
			2001			
CH_a	15	0.18 ± 0.037	0.05 ± 0.022	0.47 ± 0.104[b]	−0.05 ± 0.022[b]	
CH_b	15	0.22 ± 0.071	0.05 ± 0.027	0.54 ± 0.182	−0.04 ± 0.032	2.45
NIS_{vel}	50	0.69 ± 0.247	0.19 ± 0.114	0.51 ± 0.120[b]	−0.22 ± 0.064[b]	
NIS_{slope}	50	1.36 ± 0.484	0.09 ± 0.222	0.62 ± 0.148[b]	−0.28 ± 0.082[b]	
NIS_{combo}	50	0.64 ± 0.230	0.18 ± 0.106	0.62 ± 0.148[b]	−0.22 ± 0.082[b]	
FC	08	0.08 ± 0.021[b]	0.03 ± 0.011[b]	0.94 ± 0.150[b]	−0.02 ± 0.010[b]	
FC	15	0.15 ± 0.032[b]	0.16 ± 0.016[b]	2.50 ± 0.436[b]	−0.15 ± 0.013[b]	
SH	08	0.08 ± 0.020[b]	−0.03 ± 0.011[b]	0.07 ± 0.012[b]	0.02 ± 0.008[b]	
SH	15	0.22 ± 0.0685	0.00 ± 0.033	0.26 ± 0.075	−0.01 ± 0.030	1.18
SIS_{vel}	50	1.03 ± 0.362	0.24 ± 0.167	1.61 ± 0.635	−0.14 ± 0.1616	1.56
SIS_{slope}	50	1.31 ± 0.453	0.13 ± 0.209	1.60 ± 0.583	−0.26 ± 0.150	1.22
SIS_{combo}	50	0.95 ± 0.337	0.24 ± 0.156	1.60 ± 0.583	−0.26 ± 0.150	1.28
			2002			
FC_a	15	0.23 ± 0.067	0.02 ± 0.030	0.67 ± 0.168	−0.04 ± 0.033	2.91
FC_b	15	0.22 ± 0.079	0.07 ± 0.029	0.32 ± 0.115	−0.09 ± 0.030	1.45
FC	30	0.75 ± 0.251[b]	−0.19 ± 0.120[b]	2.16 ± 0.579[b]	0.18 ± 0.109[b]	
SR	15	0.38 ± 0.107	0.04 ± 0.052	0.68 ± 0.189	0.06 ± 0.050	1.89
SH	15	0.23 ± 0.063	0.01 ± 0.031	0.28 ± 0.077	−0.01 ± 0.030	1.22
SH	30	0.55 ± 0.161	−0.02 ± 0.080	0.77 ± 0.223[b]	0.02 ± 0.066[b]	
			2003			
LB	15	0.19 ± 0.038	0.07 ± 0.017	0.24 ± 0.052	−0.07 ± 0.017	1.33
SR	15	0.29 ± 0.073	0.02 ± 0.036	0.70 ± 0.176	0.04 ± 0.033	2.38
SH	15	0.24 ± 0.054	0.03 ± 0.026	0.28 ± 0.079	−0.02 ± 0.030	1.17

[a]All fractions (*a*) and *y* intercepts (*b*) are accompanied by their respective 95% confidence intervals. For 50 m deployments, results from all three extrapolation methods are considered included above. The ratio of the bottom transport fraction to the surface transport fraction is included as the rightmost column.
[b]Failed to meet the necessary criteria outlined in the text.

extrapolation profiles by an average of 30%. Results from the constant velocity extrapolation profiles themselves were quite variable. Using this profile, surface fractions ranged from 70 to 109% while the two significant bottom fractions were 100 and 160% respectively (Table 3). Results from the constant slope extrapolation profiles consistently overestimated the fraction of full Ekman transport present in the surface layer with all three deployments over 120%. The significant bottom transport fractions using the constant slope extrapolation method were 91% and 160% (Table 3). Results from the combined extrapolation method (constant velocity at surface, constant slope at bottom) follow those above: surface fractions were similar to the constant velocity method while bottom fractions were similar to those from the constant slope method. The high surface fractions from the constant slope extrapolation overestimate the full transport present as a result of the extrapolation method used. Both alternative methods show that the constant slope extrapolation in the bottom layer yields transport fractions only slightly different than the constant velocity extrapolation results. For these reasons, only results from the constant velocity extrapolation profiles are considered further.

[32] Using the significant results only (Table 3, Figure 5), the measured surface Ekman transport ranged from 18% to 35% of the full theoretical Ekman transport at 15 m. Measured bottom transport fractions at this depth were more variable, ranging from 25% to 70% of the full theoretical bottom Ekman transport. The surface fraction from the one significant 30 m deployment in 2002 was 55% of the full theoretical transport. Finally, as stated earlier, surface fractions at 50 m deployments ranged from 70% to 109% while bottom fractions were 100% and 160%. Viewed as a whole (Figure 5), the results from all significant deployments begin to describe the relationship between the Ekman fractions and the local water depth. In general, these results show the fraction of theoretical Ekman transport increases with offshore depth, becoming near full Ekman transport at the deepest deployment depth, 50 m. A linear fit to the surface fractions of the significant deployments increases offshore from 25% at 15 m to 90% at 50 m. A similar fit of the significant bottom fractions increases from 45% at 15 m to 130% at 50 m, although there is considerably more variability in the bottom transport fractions at both depths.

[33] As the bulk of the deployments were at water depths of 15 m, results at these locations are discussed further. At all 15 m stations except station YH, calculated bottom transport fractions were consistently larger than their corresponding surface transport fractions (Figure 6). Bottom transport fractions were an average of 1.2 and 2.1 times the surface transport fractions at stations SR and SH, 1.3 at LB, 2.5 at CH, and 2.2 at station FC while only 0.88 at YH (Table 3). Of those stations with multiple significant results in each layer, transport fractions at station FC are variable while fractions at stations SR and SH are quite steady over

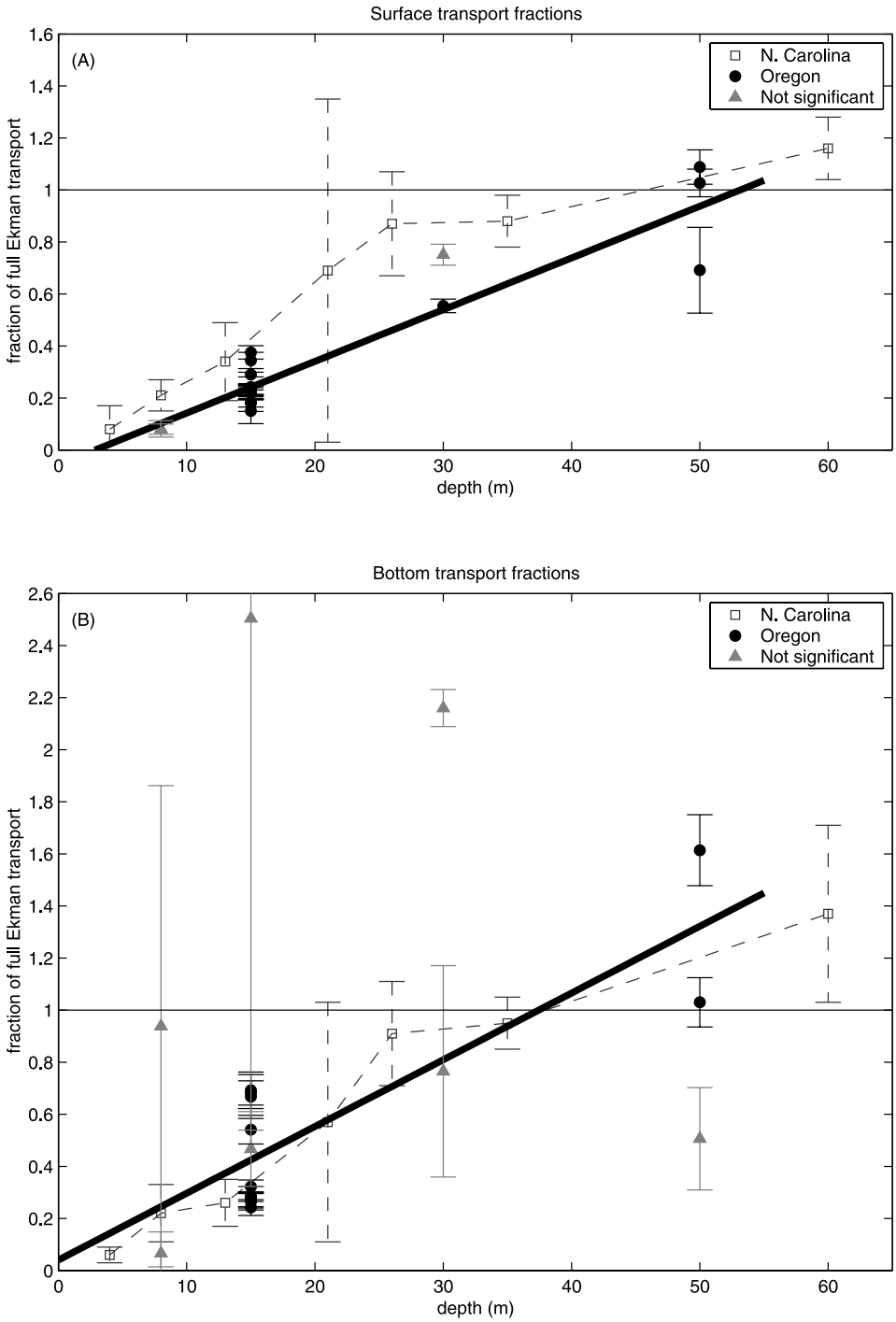

Figure 5. Fraction of full Ekman transport for (a) surface and (b) bottom transport. Filled circles indicate significant regression results, each with its individual confidence interval shown. Shaded triangles indicate the deployments that did not meet the necessary conditions for significance. A linear fit to the significant results is shown for each layer. Results for the North Carolina coast from *Lentz* [2001] are overlaid as open squares connected with a dashed line.

time. The larger bottom fractions seen here and the influence of stratification on the transport fractions are discussed in the following sections.

3.2. Effects of Bottom Stress Parameterization

[34] Assuming that the wind-driven flow is two dimensional and steady with no along-shelf pressure gradient, the depth-integrated along-shelf momentum balance is between the surface and bottom stress terms only. If this is true, the surface and bottom transport fractions should balance as well. However, results shown above give bottom fractions that are generally higher than surface fractions. In these cases, the bottom stress calculated using a frictional coefficient of $r = 5 \times 10^{-4}$ m s^{-1} was less than the surface stress

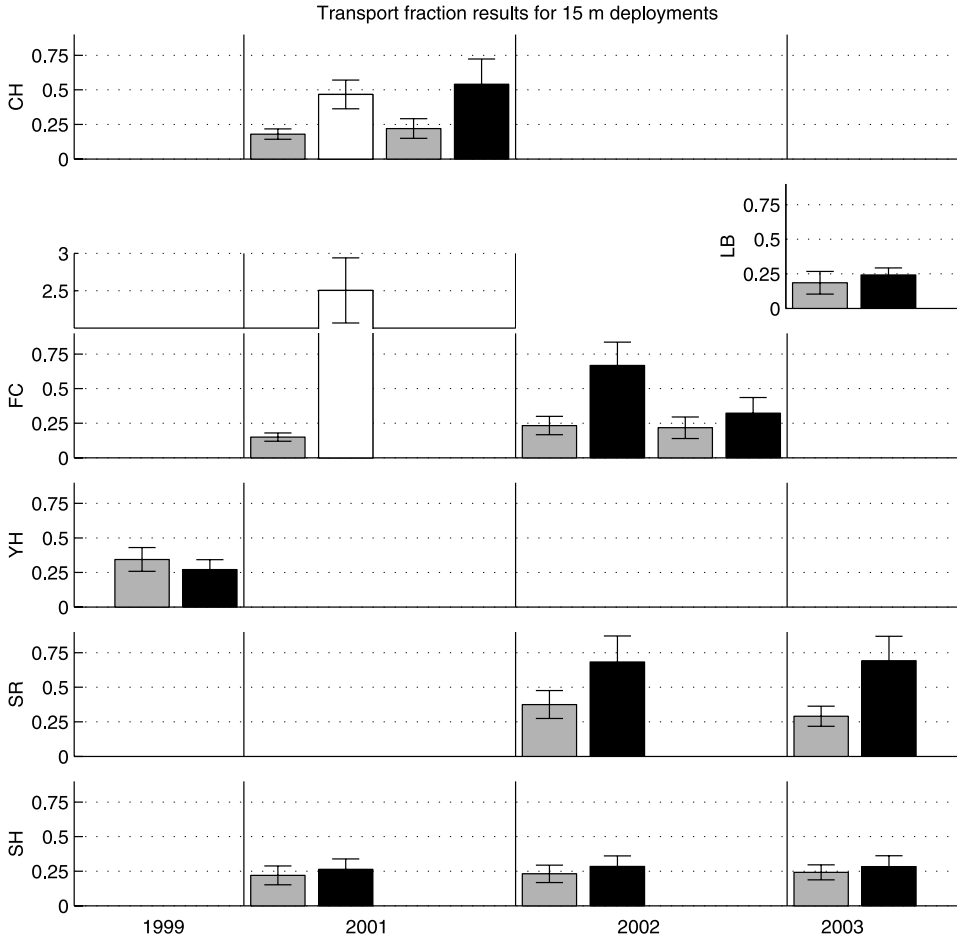

Figure 6. Transport fraction results of the 15 m deployments only. Stations are listed from north to south, and the results for each station, both surface (shaded) and bottom (filled), are displayed by deployment year, left to right. Deployment results not meeting the necessary conditions are included as well (open bars).

calculated using *Large and Pond*'s [1981] empirical relationship. Here we compute the frictional coefficient needed for bottom stress to balance surface stress by forcing the surface and bottom transport fractions to balance.

[35] Using equations (2), (4), and (6) with the above assumption that the bottom transport fraction should equal the surface transport fraction,

$$\frac{\mathrm{var}(U_b)}{R^2} = \mathrm{var}\left(r\frac{v_b}{f}\right), \tag{7}$$

where var( ) denotes a variance operation, U_b is the measured bottom transport, R is the surface transport fraction, and v_b is the bottom velocity. From this relationship, a new friction coefficient r can be found iteratively. This calculation was performed on all results, and the resulting frictional coefficients are given here as a function of both station and year (Table 4) and of local water depth (Figure 7). At most deployments the calculated coefficients are greater than the original value of $r = 5 \times 10^{-4}$ m s^{-1}. A linear fit to the calculated frictional coefficients increases slightly with decreasing depth from 7×10^{-4} at 50 m depth to 9×10^{-4} at 15 m depth. At 50 m, the new value of r is close to the initial value used, while an average 1.7 times the original value is needed at 15 m. However, the range of the calculated coefficients at 15 m is quite large, spanning an order of magnitude. The variability of r could be due to terms in momentum balance we have neglected here, however the increase of r with decreasing water depth is consistent with an increase in bottom stress due to the effect of surface gravity waves in the bottom boundary layer [*Grant and Madsen*, 1979].

3.3. Influence of Stratification

[36] As mentioned earlier, observations and model studies indicated reduced Ekman transport at lower levels of stratification. Decreasing stratification acts to thicken the boundary layers, as stratification affects the eddy viscosity in the Ekman velocity derivation [*Allen et al.*, 1995; *Austin and Lentz*, 2002]. Because the surface and bottom boundary layers overlap in the inner shelf, changes in stratification should have a direct effect on the fraction of full Ekman transport present.

[37] A simple example of decreases in the fraction of full Ekman transport occurring at the same time as reductions in stratification was observed at station YH, a 15 m deployment made in 1999. Using the top-to-bottom temperature gradient as a proxy for the density stratification, the stratification decreased over the deployment period

Table 4. Calculated Bottom Friction Coefficients Found by Matching the Surface and Bottom Transport Fractions[a]

Station	Depth, m	Duration, days	r, 10^{-4} m s^{-1}
		1999	
YH	15	67	4
IS	50	77	5
		2001	
CH	15	80	NA
	15	50	12
NIS	50	104	NA
FC	08	100	NA
	15	62	NA
SH	08	46	NA
	15	63	6
SIS	50	105	9
		2002	
FC	15	62	14
	15	33	7
	30	51	NA
SR	15	115	9
SH	15	111	6
	30	52	NA
		2003	
LB	15	111	7
SR	15	116	12
SH	15	122	6

[a]The coefficients are included only for those deployments where both the bottom and surface transport fractions meet the necessary conditions. Deployments failing these conditions are marked as NA, not applicable. Compared to the original value of $r = 5 \times 10^{-4}$ m s^{-1}, the results of this calculation are larger and increase in magnitude with decreasing local depth. NA, not applicable.

(Figure 8). The effect of stratification on the cross-shelf transport is apparent if we divide the transport results into two regimes, an initial stratified regime and a more weakly stratified regime occurring after early September (year day 250), and then perform the neutral regression analysis described earlier on both halves. With a mean gradient of 0.19°C m^{-1}, in the stratified regime the surface transport fraction was 38% while the bottom transport fraction was 33%. In contrast, during the weakly stratified regime, with a mean gradient of 0.09°C m^{-1}, both the surface and bottom transport fractions were reduced to 31% and 24% respectively.

[38] To test this hypothesis further, the fraction of full transport and average stratification were compared over shorter time intervals for the surface layers of all 15 m deployments. The measured and theoretical Ekman transports were used to compute the transport fractions in incremental 6 day blocks. Then the transport fractions were compared to the average stratification of each time block. A scatterplot (Figure 9) of the average stratification and surface transport fraction time series from all deployments suggests a weak linear dependence. A neutral regression of the surface transport fraction and average stratification time series gives a slope and intercept of 2.5 and near 0 respectively. Thus using the full surface layer data set yields a stronger dependence of transport fraction on stratification than in the single YH 15 m example (Figure 8).

4. Discussion

[39] The results of the Ekman transport calculation presented above clearly illustrate the offshore divergence of Ekman transport in the inner shelf off Oregon. The wind-driven dynamics that control circulation offshore appear to extend inshore with a magnitude adjustment based on the divergence of Ekman transport along a coastal boundary. Yet the role of wind stress curl in this process and the wind-driven dynamics in water less than 15 m depth deserve further discussion. In addition, we will compare these results to previous studies and discuss the validity of using temperature differences as a proxy for density stratification on the inner shelf.

4.1. Wind Stress Curl

[40] In contrast to a number of previous studies, wind stress curl is unlikely to be significant cause of upwelling in

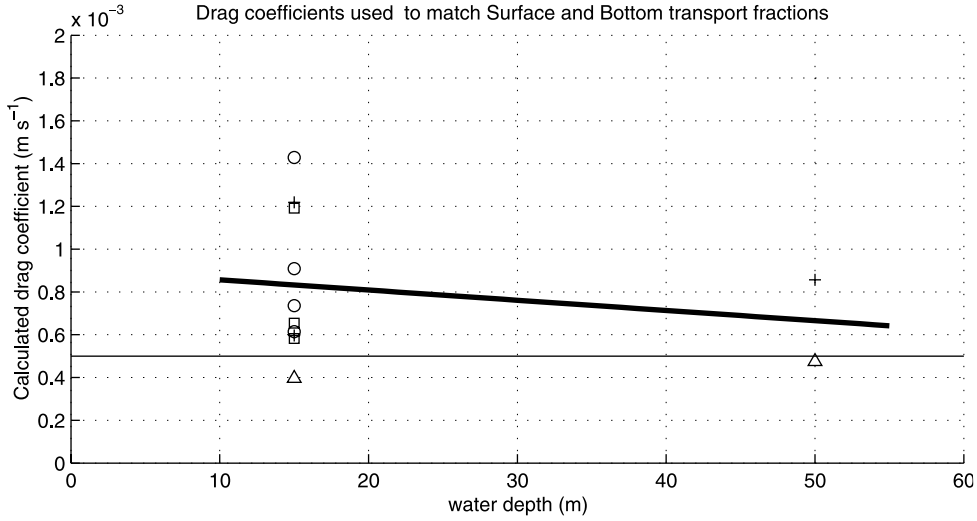

Figure 7. Bottom drag coefficient found by requiring the bottom transport fraction to equal the surface transport fraction. Calculated coefficients are shown for all deployments where results from both layers were significant. A linear fit to the results shows a trend of increasing r values with decreasing water depth. The year of each deployment is noted: 1999, triangles; 2001, crosses; 2002, circles; and 2003, squares.

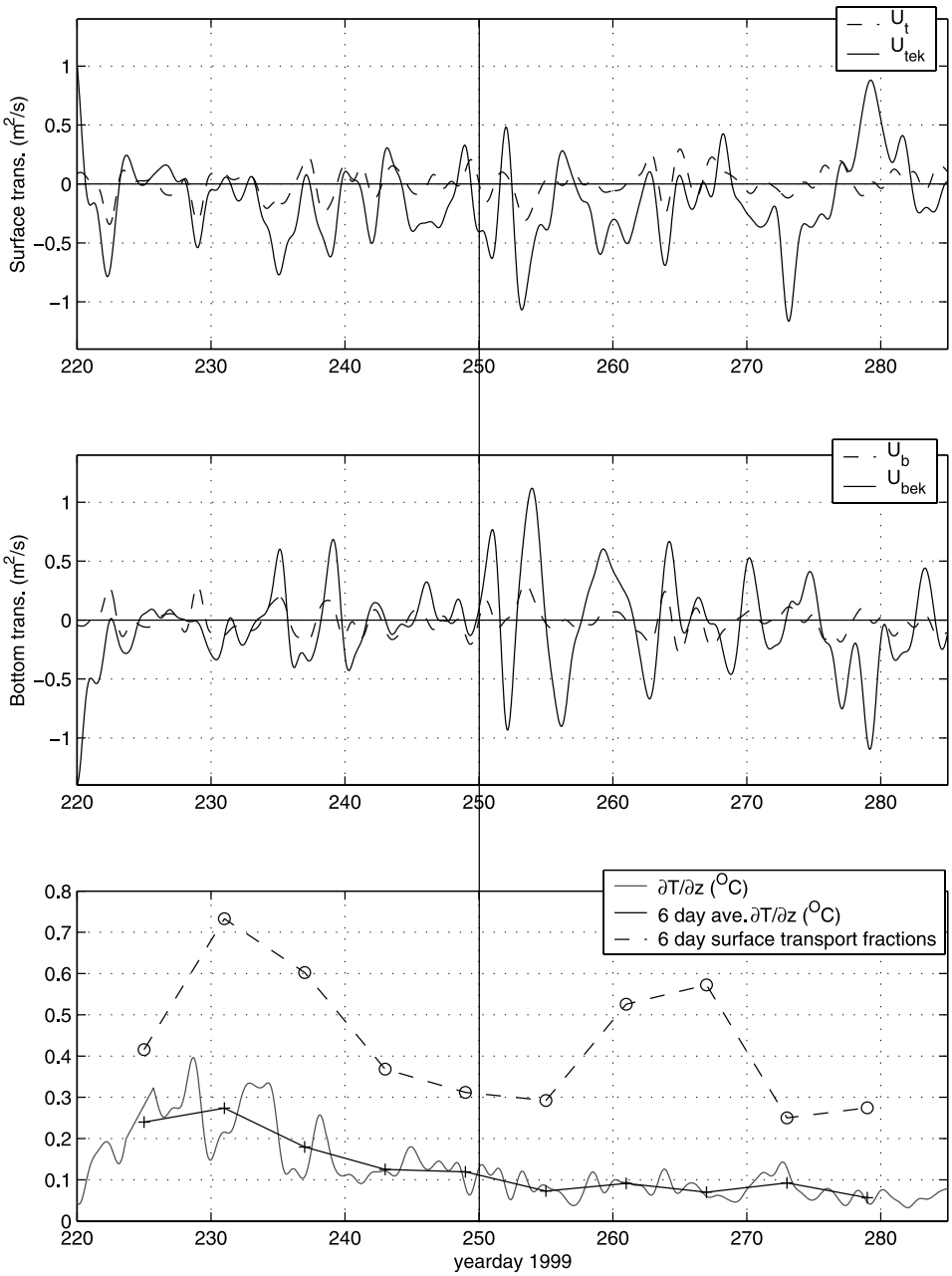

Figure 8. Stratification and transport results for the 15 m deployment at station YH in 1999. Resulting measured (U_t and U_b) and theoretical (U_{tek} and U_{bek}) Ekman transport for both the (top) surface layer and the (middle) bottom layer. (bottom) Stratification proxy, the 6 day block averages of stratification, and the 6 day surface transport fractions. The decrease of transport fractions with decreased stratification is visually seen by comparing the measured and theoretical transport before and after year day 250.

the inner shelf off central Oregon. As shown here, CMAN station winds were at least 80% of the magnitude of winds measured offshore at buoy 46050. Small cross-shelf and along-shelf curl was also reported by *Samelson et al.* [2002] for our study area. In contrast, *Lentz* [1994] reported large wind stress curl for the CODE region off northern California. In that region, along-shelf wind speeds 1 km offshore (at 30 m depth) were 1/3 the magnitude of along-shelf wind speeds 8 km offshore (at 90 m depth) [*Lentz*, 1994]. Our results also contrast with the recent model results of Ekman transport and pumping given by *Pickett and Paduan* [2003] for the continental shelf off central California where pumping caused a significant fraction of the total upwelling velocity. The differences from this study are twofold. First, *Pickett and Paduan* [2003] measured significant wind stress curl (up to 10^{-5} N m^{-3}) within 50 km of the coast, highest downwind (equatorward) of coastal promontories. Off Oregon, the maximum cross-shelf curl measured here was much less at $\sim 10^{-6}$ N m^{-3} (Table 2). Second, *Pickett and Paduan* [2003] used a Rossby radius of 10 or 20 km to convert

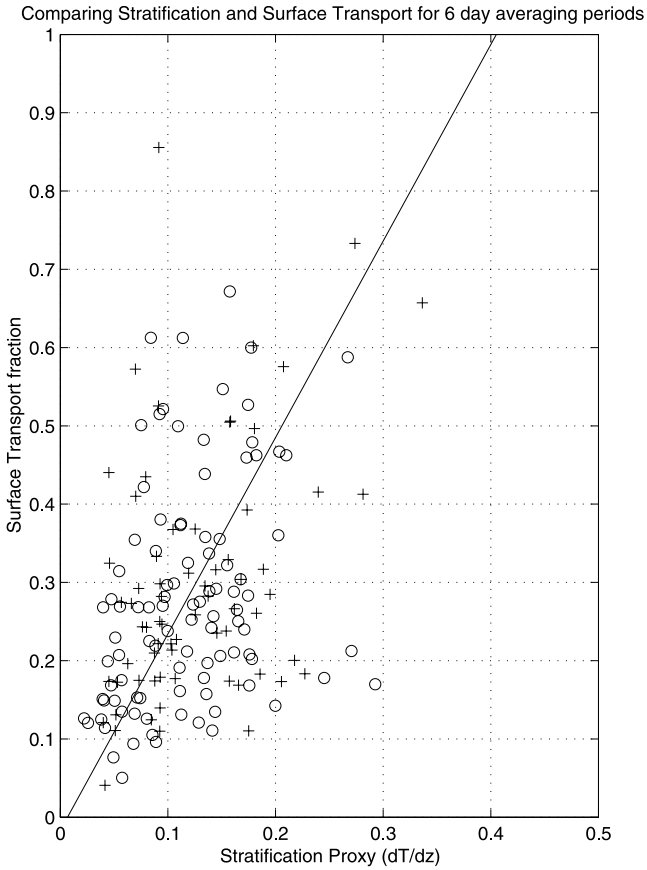

Figure 9. Scatterplot of 6 day block average stratification and 6 day block surface transport fractions from the 15 m deployments. Stratification averages were found using the 1–14 m temperature differences (circles) or the 4–14 m temperature differences (crosses). A neutral regression of stratification versus transport fraction gives a slope and intercept of 2.5 and −0.01, respectively. The two time series are weakly positively correlated, having a correlation coefficient of 0.35 with a 95% level of significance of 0.17. The correlation was strongest using the 6 day averaging interval shown here, i.e., the middle of the weather band.

Ekman transports into upwelling velocities. The resulting vertical velocity was found to be of the same order as the Ekman pumping velocity which peaks at about 25 km offshore. As shown here from the Ekman divergence off central Oregon, upwelling is fully realized by a water depth of 50 m or 4–5 km offshore (Figure 2). This value is significantly shorter than the 10–20 km used by *Pickett and Paduan* [2003] and would result in higher vertical velocities.

4.2. Comparing With Previous Results

[41] Comparing the transport fraction results presented here with those reported by *Lentz* [2001] for the wide North Carolina shelf indicates a dynamical similarity between the two regions. Overlaying the two series (Figure 5), the results from North Carolina fall close to those from Oregon in both layers but have consistently higher surface transport fractions. These similarities are notable given the large difference in shelf geometry. Off Oregon, 15 m moorings were 1 km offshore while 50 m locations were about 5 km offshore. In contrast, off North Carolina, the 13 m site was 1.6 km offshore while the 60 m site was 77 km offshore. Thus results from the two areas collapse when compared by water depths, but are quite different when compared by offshore distance. In addition, the 5 km offshore extent of Ekman divergence found here is half the value reported by *Huyer* [1983] using midshelf measurements made off central Oregon.

[42] Using combination of current meters and ADCPs, Austin and Grantham (submitted manuscript, 2005) reported cross shelf transport fraction results for additional PISCO mooring locations in 1999 and 2000. With a similar method, the authors found surface transport fractions at station SH of 25% and 16% in 1999 and 2000 respectively. Their results concur with those seen here, indicating the steady nature of the wind-driven dynamics at this station over the course of six summers. However, like those reported here, fractions from station FC were quite variable. The variability seen at station FC will be discussed in the next section.

4.3. Calculation Failures

[43] Given the cross-shelf divergence of Ekman transport found on the Oregon inner shelf and its similarities to the cross-shelf transports observed elsewhere, those deployments that failed to meet the necessary conditions are of further interest as they raise questions about the assumptions used in this analysis. Notable failures of the transport calculations occurred in all measurements taken at 8 m locations and at more than half the deployments made at station FC. These deployments failed as either the measured transports were uncorrelated with the stresses or a significant wind-driven depth-averaged cross-shelf velocity component existed. Again, positive correlations of the measured transports and stresses and no significant correlation between the surface stress and the depth-averaged cross-shelf velocity are necessary conditions of the theory used here.

[44] We suggest that the influence of local bathymetry is responsible for the failure of the transport calculations at station FC. The rotation of the principal axis of flow with depth for deployments at station FC are significantly higher than any other station. The range of principal axis orientations spanned 80° and 71° for the 2001 deployments at 15 and 8 m, 43° and 21° for the 2002 15 m deployments, and 43° for the 30 m deployment in 2002 (Table 1). Comparatively, the 30 m deployment at station SH had a total range of 10° (Table 1). A wide range of turning with depth (40°–70°) in 15 m indicates the assumption of along-shelf uniformity and two-dimensional flow might not be valid at this location. Indeed, station FC is located just north of a headland (Figure 1), possibly causing this variability. In contrast, station LB located a few kilometers farther north in a region of smoother topography has a principal axis range of only 7°. Further, correlations of the depth-averaged along-shelf velocities from all years (not shown here) found that currents at station FC were poorly correlated with all other stations, even though stations to the north and south were well correlated. These results indicate that a systematic difference between station FC and stations both to the north and south exists, most likely the result of local bathymetry.

[45] In addition to the transport calculation failure for the FC 8 m deployment, inconsistent results occurred for the SH 8 m deployment as well. Given the shallow water depth of these deployments, a large fraction of the water column (37%) was not measured by the instruments. Velocities in these regions (2 m at bottom and 1 m at top) were assumed by extrapolation and remain a possible source of error in the transport calculation. In addition, we hypothesize that these mooring locations were frequently in the surf zone where wave-induced radiation stresses can be a dominant force. If true, root mean squared wave heights (H_{rms}) must be large enough to cause wave breaking and dissipation at the mooring location, resulting in nonzero wave radiation stresses in the depth-averaged along-shelf momentum balance. During the period of the 8 m deployments, H_{rms} wave heights measured offshore at buoy 46050 averaged 2 m with peak wave heights exceeding 3–4 m. With similar H_{rms} wave heights, *Lentz et al.* [1999] observed the surf zone extending past an 8 m mooring location on a number of occasions off North Carolina. Even though appropriate measurements (i.e., wave direction) to fully investigate this point were not made in our study, the results raise questions about the exact nature of the cross-shelf transport that occurs between the surf zone and the inner shelf.

4.4. Temperature Difference and Stratification

[46] Our analysis links the level of stratification to the cross-shelf transport fractions using the top to bottom temperature difference, divided by the depth between them, as a proxy for the actual density stratification present. However, density over the Oregon shelf is also a strong function of salinity. Thus it is necessary to determine how well temperature works as a proxy for density. If temperature changes throughout the water column are well correlated with salinity changes, we would have reason to assume that temperature is a good predictor of density.

[47] Where we have salinity measurements (8 m depth at each 15 m mooring), salinity is strongly negatively correlated with temperature (Table 5). Further, correlating the 8 m salinity with temperature measurements from all available depths showed that temperatures throughout the water column were negatively correlated with the 8 m salinity at most locations (Table 5). In fact, only a few examples exist in the data where the surface temperature is not significantly correlated to the 8 m salinity. While surface heating might be a factor in these few examples, this simple test indicates that temperature and salinity generally fluctuate together over the entire water column at these shallow inner-shelf stations. Conductivity-temperature-depth (CTD) casts (not shown here) made by the PISCO program adjacent to most mooring locations further support this result. In most casts, observed temperature and salinity gradients are colocated with warm, fresh water overlaying cold, salty waters. Therefore the top-to-bottom temperature difference used here is a valid proxy for the density stratification present over the inner shelf during summer.

Table 5. Correlation Coefficients (CC) Between 8 m Salinity and Temperature Measurements From All Depths for 15 m Deployments[a]

Station	Depth, m	Duration, days	CC
	1999		
YH	3	44	−0.833
	8	89	−0.646
	13	89	−0.752
	2001		
CH	1	110	−0.648
	4	140	−0.704
	9	140	−0.776
	14	140	−0.731
FC	1	81	−0.730
	4	125	−0.787
	9	65	−0.800
	14	121	−0.808
SR	1	105	−0.625
	4	133	−0.707
	9	133	−0.763
	14	133	−0.758
SH	1	60	−0.767
	4	103	−0.636
	9	103	−0.752
	14	103	−0.771
	2002		
FC	9	71	−0.915
	14	71	−0.914
SR	1	111	−0.735
	4	111	−0.780
	9	111	−0.893
	14	111	−0.908
SH	1	87	−0.473
	4	87	−0.554
	9	87	−0.655
	14	87	−0.707
	2003		
LB	1	111	−0.705
	4	120	−0.784
	9	120	−0.813
	14	120	−0.768
SR	1	63	−0.592[b]
	4	116	−0.796
	9	116	−0.847
	14	116	−0.854
SH	1	120	−0.716
	4	120	−0.749
	9	90	−0.731
	14	120	−0.691

[a]All time series used were band-pass filtered prior to computing the correlation coefficients, isolating variability with periods from 2 to 10 days. This technique was employed to remove larger-amplitude unresolved seasonal trends, maximizing the effective degrees of freedom in the correlations.

[b]Not significant at the 95% confidence level.

4.5. Implications for Larval Transport and Phytoplankton Blooms

[48] Our results have several ecological implications. The first is that our data suggest cross-shelf transport of materials such as larvae and phytoplankton may be minimal inshore of about 15 m depth. Two observations are consistent with this interpretation. Barnacle (*Balanus glandula* and *Chthamalus dalli*) recruitment varies little with latitude along the stretch of coast encompassed by the PISCO mooring array [*Menge et al.*, 2002]. In the context of the present results that indicate little cross-shelf Ekman transport occurs inshore of 15 m depth, barnacle larvae released into inner-shelf waters may be retained there rather than being swept far offshore as has been suggested for California coastal waters [e.g., *Roughgarden et al.*, 1988; *Farrell et al.*, 1991]. Since we find no evidence for a latitudinal pattern in the cross-shelf width of the divergence

of Ekman transport, if barnacle larvae tend to remain within or inshore of this band, no latitudinal trend in barnacle recruitment would be expected.

[49] A second observation consistent with our interpretation is the regular observation of sharp color fronts between the near shore and waters 1–2 km offshore. We have regularly observed these fronts on PISCO cruises and other work in the region. Water samples from shore and ship-based surveys indicate that the difference in color is caused by dense coastal phytoplankton blooms (that color the water brown) abutting offshore waters (green in color) with much lower phytoplankton concentrations. Whether or not this front represents the outer edge of the region our physical measurements have identified as the region of reduced cross-shelf transport in the inner shelf is not known and bears further investigation.

[50] Finally, observed recruitment patterns suggest that the link between cross-shelf transport and larval dispersal (or retention) in the inner shelf may vary at a larger latitudinal scale. Data on geographic variation in barnacle recruitment indicates that, in contrast to the minimal variation in recruitment seen along the central Oregon coast, recruitment varies enormously between regions north and south of Cape Blanco, on the southern Oregon coast [*Connolly et al.*, 2001; *Menge et al.*, 2004]. Recruitment rates are high north of Cape Blanco, while south of the Cape and throughout California, recruitment rates are significantly lower. These data and the results of this study imply that a fundamental difference in the link between cross-shelf transport and larval dispersal (e.g., differences in the near-shore stratification or wind stress patterns) exists north and south of the Cape, causing higher offshore losses of larvae to the south. This hypothesis deserves further research.

5. Conclusions

[51] The fraction of the full theoretical Ekman transport present in the wind-driven cross-shelf circulation over the Oregon inner shelf increased from 25% of full Ekman transport at 15 m depth (1–2 km offshore) to full Ekman transport near 50 m depth (5–6 km offshore). In general, transport fractions were found to be locally steady at those stations occupied for multiple years. The assumption of along-shelf uniformity was found to hold at most locations and velocities at these stations were well correlated along the coast. At station FC, the consistent exception to most results reported here, velocity profiles from all deployments exhibit significant turning of the principal axis of flow with depth. This indicates flow at this location is significantly influenced by local along-shelf bathymetric variations, causing deviations from theoretical Ekman predictions.

[52] The preliminary drag coefficient assumed here in the linear bottom stress parameterization resulted in bottom transport fractions that were consistently higher than surface transport fractions. Adjusting this coefficient to balance the bottom and surface transport fractions resulted in slightly higher drag coefficients that increased in magnitude moving onshore. This increase is consistent with higher drag near-shore due to surface gravity wave effects on the bottom boundary layer.

[53] The fraction of full Ekman transport as a function of water depth found here is similar to that reported by *Lentz* [2001] for the wide North Carolina coast. Thus the region of Ekman divergence is dependent on local water depth rather than offshore distance. Additionally, a comparison of the 6 day average stratification and surface transport fractions showed that the level of stratification was weakly correlated with and linearly related to the fraction of cross-shelf transport. A reduction of stratification would act to thicken the boundary layers and increase the boundary layer depth overlap in shallow waters by increasing the eddy viscosity. This process was suggested by *Lentz* [2001] and modeled by *Austin and Lentz* [2002] as leading to a shutdown of the inner-shelf circulation. Finally, reduced cross-shelf transport in the inner shelf could suppress the connection between the shore and the mid shelf, leading to retention of organisms within the inner shelf.

[54] **Acknowledgments.** The authors would like to acknowledge the David and Lucile Packard Foundation for its support of the PISCO mooring program at OSU. M. Levine and T. Boyd generously provided the NOPP (Office of Naval Research Grant N00014-98-1-0787) and COAST (National Science Foundation Grant OCE-9907854) 50 m mooring and meteorological data used in this analysis. We thank M. Levine and J. Austin (of Old Dominion University) for helpful discussions. This work was supported in part by NSF grant OCE-9907854. This paper is PISCO contribution 161.

References

Allen, J. A., and R. Smith (1981), On the dynamics of wind-driven shelf currents, *Philos. Trans. R. Soc. London, Ser. A*, *302*, 617–634.

Allen, J. A., P. A. Newberger, and J. Federick (1995), Upwelling circulation on the Oregon continental shelf, part 1: Response to idealized forcing, *J. Phys. Oceanogr.*, *25*, 1843–1866.

Austin, J. A., and S. J. Lentz (2002), The inner shelf response to wind-driven upwelling and downwelling, *J. Phys. Oceanogr.*, *32*, 2171–2193.

Boyd, T., M. D. Levine, P. M. Kosro, and S. R. Gard (2000), Mooring observations from the Oregon continental shelf: April–September 1999, *Data Rep. 177, Ref. 2000-1*, Oreg. State Univ., Corvallis.

Boyd, T., M. D. Levine, P. M. Kosro, S. R. Gard, and W. Waldorf (2002), Observations from moorings on the Oregon continental shelf: May–August 2001, *Data Rep. 190, Ref. 2002-6*, Oreg. State Univ., Corvallis.

Connolly, S. R., B. A. Menge, and J. Roughgarden (2001), A latitudinal gradient in recruitment of intertidal invertebrates in the northeast Pacific Ocean, *Ecology*, *82*, 1799–1813.

Ekman, V. W. (1905), On the influence of the Earth's rotation on ocean-currents, *Arkiv Math. Astro. Fys.*, *2*, 1–53.

Farrell, T. M., D. Bracher, and J. Roughgarden (1991), Cross-shelf transport causes recruitment to intertidal populations in central California, *Limnol. Oceanogr.*, *36*, 279–288.

Feddersen, F., R. T. Guza, S. Elgar, and T. H. C. Herbers (1998), Alongshore momentum balances in the nearshore, *J. Geophys. Res.*, *103*, 15,667–15,676.

Garrett, C., and B. Petrie (1981), Dynamical aspects of the flow through the Strait of Belle Isle, *J. Phys. Oceanogr.*, *11*, 376–393.

Gill, A. (1982), *Atmosphere-Ocean Dynamics*, Elsevier, New York.

Gordon, R. L. (1996), Acoustic Doppler current profiler: Principles of operation, a practical primer, second edition for broadband ADCPs, report, RDI Instruments, San Diego, Calif.

Grant, W. D., and O. S. Madsen (1979), Combined wave and current interaction with a rough bottom, *J. Geophys. Res.*, *84*, 1797–1808.

Hickey, B. M. (1998), Coastal oceanography of western North America from the tip of Baja California to Vancouver Island, in *The Sea*, vol. 11, edited by A. R. Robinson and K. H. Brink, chap. 12, pp. 345–393, John Wiley, Hoboken, N. J.

Huyer, A. (1983), Coastal upwelling in the California current system, *Prog. Oceanogr.*, *12*, 259–284.

Huyer, A. (1990), Shelf circulation, in *The Sea*, vol. 9A, edited by B. LeMehaute and D. M. Hanes, chap. 12, pp. 1647–1658, John Wiley, Hoboken, N. J.

Large, W. G., and S. Pond (1981), Open ocean momentum flux measurements in moderate to strong winds, *J. Phys. Oceanogr.*, *11*, 324–336.

Lentz, S. J. (1992), The surface boundary layer in coastal upwelling regions, *J. Phys. Oceanogr.*, *22*, 1517–1539.

Lentz, S. J. (1994), Current dynamics over the northern California inner shelf, *J. Phys. Oceanogr.*, *26*, 2461–2478.

Lentz, S. J. (1995), Sensitivity of the inner-shelf circulation to the form of the eddy viscosity profile, *J. Phys. Oceanogr.*, *25*, 19–28.

Lentz, S. J. (2001), The influence of stratification on the wind-driven cross-shelf circulation over the North Carolina shelf, *J. Phys. Oceanogr.*, *31*, 2749–2760.

Lentz, S. J., and J. H. Trowbridge (1991), The bottom boundary layer over the northern California shelf, *J. Phys. Oceanogr.*, *21*, 1186–1200.

Lentz, S. J., and C. D. Winant (1986), Subinertial currents on the southern California shelf, *J. Phys. Oceanogr.*, *16*, 1737–1750.

Lentz, S. J., R. T. Guza, S. Elgar, F. Feddersen, and T. H. C. Herbers (1999), Momentum balances on the North Carolina inner shelf, *J. Geophys. Res.*, *104*, 18,205–18,226.

MacCready, P., and P. B. Rhines (1993), Slippery bottom boundary layers on a slope, *J. Phys. Oceanogr.*, *23*, 5–22.

Menge, B. A., E. Sanford, B. A. Daley, T. L. Freidenburg, G. Hudson, and J. Lubchenco (2002), An inter-hemispheric comparison of bottom-up effects on community structure: Insights revealed using the comparative-experimental approach, *Ecol. Res.*, *17*, 1–16.

Menge, B. A., C. Blanchette, P. Raimondi, S. Gaines, J. Lubchenco, D. Lohse, G. Hudson, M. Foley, and J. Pamplin (2004), Species interaction strength: Testing model predictions along an upwelling gradient, *Ecol. Monogr.*, *74*, 663–684.

Mooers, C. N. K. (1968), A compilation of observations from moored current meters and thermographs, vol 2: Oregon continental shelf, August–September 1966, *Data Rep. 68-5*, Oreg. State Univ., Corvallis.

Morgan, S. G. (2001), The larval ecology of marine communities, in *Marine Community Ecology*, edited by M. D. Bertness, S. D. Gaines, and M. E. Hay, pp. 159–181, Sinauer, Sunderland, Mass.

Oke, P. R., J. S. Allen, R. N. Miller, G. D. Egbert, J. A. Austin, J. A. Barth, T. J. Boyd, P. M. Kosro, and M. D. Levine (2002), A modeling study of the three-dimensional continental shelf circulation off Oregon. Part 1: Model-data comparisons, *J. Phys. Oceanogr.*, *32*, 1360–1382.

Pickett, M. H., and J. D. Paduan (2003), Ekman transport and pumping in the California Current based on the U.S. Navy's high-resolution atmospheric model (COAMPS), *J. Geophys. Res.*, *108*(C10), 3327, doi:10.1029/2003JC001902.

Reed, B. C. (1992), Linear least-squares fits with errors in both coordinates, *Am. J. Phys.*, *60*, 59–62.

Roughgarden, J., S. D. Gaines, and H. Possingham (1988), Recruitment dynamics in complex life cycles, *Science*, *241*, 1460–1466.

Samelson, R. M. (1997), Coastal boundary conditions and the baroclinic structure of wind-driven continental shelf currents, *J. Phys. Oceanogr.*, *27*, 2645–2662.

Samelson, R., et al. (2002), Wind stress forcing of the Oregon coastal ocean during the 1999 upwelling season, *J. Geophys. Res.*, *107*(C5), 3034, doi:10.1029/2001JC000900.

Small, L. F., and D. W. Menzies (1981), Patterns of primary productivity and biomass in a coastal upwelling region, *Deep Sea Res.*, *28*, 123–149.

Smith, R. L. (1995), The physical processes of coastal ocean upwelling systems, in *Upwelling and the Ocean: Modern Processes and Ancient Records*, edited by C. P. Summerhayes et al., pp. 39–64, John Wiley, Hoboken, N. J.

Winant, C. D. (1980), Downwelling over the southern California shelf, *J. Phys. Oceanogr.*, *10*, 791–799.

J. A. Barth and A. R. Kirincich, College of Oceanic and Atmospheric Sciences, 104 Ocean Administration Building, Oregon State University, Corvallis, OR 97331, USA. (barth@coas.oregonstate.edu; akirinci@coas.oregonstate.edu)

B. A. Grantham, Washington State Department of Ecology, Coastal and Estuarine Assessment Unit, P.O. Box 47600, Olympia, WA 98504, USA. (bgra461@ecy.wa.gov)

J. Lubchenco and B. A. Menge, Department of Zoology, Cordley 3029, Oregon State University, Corvallis, OR 97331, USA. (lubchenco@science.oregonstate.edu; mengeb@oregonstate.edu)